Int. J. Electrochem. Sci., 17 **(2022)** Article Number: 22041, doi: 10.20964/2022.04.56

International Journal of
ELECTROCHEMICAL
SCIENCE
www.electrochemsci.org

Influence of KNO_3 on Capacitive Properties of Active Carbon in Potassium Ferricyanide Solutions

Huaning Jiang[1,2], *Ying Tian*[1,2,*] , *Ming Liu*[2], *Xiaohui Zhou*[2], *Rong Xue*[3]

[1] Department of Materials and Science Engineering, Dalian Jiaotong University, Dalian 116028, P. R. China;
[2] Key Laboratory of Environmental Science and Technology, Education Department of Liaoning Province, College of Environmental and Chemical Engineering, Dalian Jiaotong University, Dalian 116028, P. R. China;
[3] Dalian Nationalities University, School of Physics & Materials Engineering, Dalian 116600, P. R. China.
[*]E-mail: greenhusk.tian@outlook.com

Received: 23 August 2021 / *Accepted:* 10 January 2022 / *Published:* 4 March 2022

Electrolyte plays an integral role in electrochemical capacitors with active carbon electrodes. A critical challenge in electrolyte formula is to achieve a decent balance between voltage window and capacitance of the capacitor. In this study, redox-active aqueous electrolytes, which consist of neutral KNO_3 aqueous solution and $K_4[Fe(CN)_6]$, were used to extend the voltage window of active carbon (AC) capacitors and improve their performance. Cyclic voltammetry test, galvanostatic charge-discharge test and electrochemical impedance spectroscopy test were conducted to investigate the pseudocapacitive effects of KNO_3-$K_4[Fe(CN)_6]$ on AC electrodes, which were respectively arranged in three-electrode and two-electrode capacitor configuration. Faradaic redox reactions of $[Fe(CN)_6]^{3-}$/$[Fe(CN)_6]^{4-}$ occurred on the positive electrodes. The working voltage window of the electrodes in the neutral electrolyte was larger than that in the control electrolyte, resulting in considerable performance enhancement. The specific capacitance, power density and energy density respectively reached 250 F g^{-1}, 332 W kg^{-1} and 14.4 Wh kg^{-1} at a current density of 1.0 A g^{-1} in the redox-active aqueous electrolyte for a symmetric AC capacitor. The most favorable balance among energy density, power density and cycle life was realized when the $K_4[Fe(CN)_6]$ concentration was 0.033 M.

Keywords: Potassium ferricyanide; voltage window; active carbon; neutral electrolyte; redox reaction

1. INTRODUCTION

Electrochemical capacitors have various superiorities, such as high power density and long cycle life. They have recently attracted increasing attention because of their potential applications in electric

devices and vehicles [1-3]. Carbon-based materials are considered the most crucial candidates in supercapacitor manufacturing as they feature low cost, favorable electrical conductivity and excellent durability. However, their specific capacitance is low, and the energy density is still unsatisfactory. Surface functionalizing carbon-based materials, which attaches carbonyl, hydroxyl and quinone groups on the surface, can lead to quick Faradaic reactions, further ameliorating their properties [4-8]. Nevertheless, the functionalities often display unsatisfactory stability in charging-discharging cycling. This significantly limits the practical application of surface modification of carbon-based materials in production [9,10].

One alternative method for increasing the energy storage capacity of carbon-based materials is using redox additives or redox-active electrolytes. Possible choices are various inorganic redox couples and organic redox mediators. One of the most representative of them is the redox pair of $Fe(CN)_6^{3-}$ /$Fe(CN)_6^{4-}$ which has excellent reversibility. For example, in an electrolyte of 1 M KOH with $Fe(CN)_6^{3-}$ /$Fe(CN)_6^{4-}$, double specific capacitance of reduced graphene oxide electrode can be achieved, compared to the control in the electrolyte without $Fe(CN)_6^{3-}$/$Fe(CN)_6^{4-}$ [11]. Similarly, adding $K_3[Fe(CN)_6]$ in an electrolyte of 1 M KOH results in an outstanding capacitance of 7514 F g^{-1} for a grapheme/$Co(OH)_2$ electrode [12]. Whereas adding $Fe(CN)_6^{3-}$/$Fe(CN)_6^{4-}$ into an electrolyte of 1 M H_2SO_4 brings about a specific capacitance as high as 912 F g^{-1} for polyaniline electrode compared to the 100 F g^{-1} in control [13]. However, these high specific capacitances are obtained in a three-electrode system, which is constantly nonequivalent with the properties in a practical two-electrode capacitor configuration because of their vastly different potential windows during the charge-discharge processes. For carbon-based materials in a two-electrode capacitor configuration, it is still very challenging to increase their specific capacitance and energy density in a $Fe(CN)_6^{3-}$/$Fe(CN)_6^{4-}$ electrolyte.

The energy density (*E*) can be calculated by $E = \frac{1}{2}cV^2$, according to which *E* can be increased by enhancing cell capacitance (*c*), voltage window (*V*) or the combination of both. At present, many researchers have proposed to employ acidic H_2SO_4 or alkaline KOH with $Fe(CN)_6^{3-}$/$Fe(CN)_6^{4-}$ couple to obtain high specific capacitances [11-13]. However, this measure can limit the potential window of the supercapacitor system to below 1.0 V because the theoretical decomposition potential of water is 1.23 V. On the other hand, some neutral mediums (*e.g.*, Na_2SO_4, $LiSO_4$, and $LiNO_3$) have successfully widened the working potential window to 1.5-2.0 V, which further significantly elevates the energy density [14-20]. In the previous reports, little attention has been paid to increasing energy density via widening the voltage window and raising cell capacitance. Based on these considerations, in this study, the $Fe(CN)_6^{3-}$/$Fe(CN)_6^{4-}$ redox-active couple was added in a neutral electrolyte, and a two-electrode capacitor configuration was used. Such arrangement was expected to widen the working potential window and increase the cell capacitance by redox reactions simultaneously, and thus significantly enhance the super capacitive performances. A neutral medium of KNO_3 and $K_4[Fe(CN)_6]$ with various concentrations was mixed to obtain a redox aqueous electrolyte. KNO_3-$K_4[Fe(CN)_6]$ and active carbon materials were used in both a three-electrode configuration and a two-electrode capacitor configuration. Cyclic voltammetry (CV) test, galvanostatic charge-discharge test and electrochemical impedance spectroscopy (EIS) test were carried out to investigate their electrochemical properties and

pseudocapacitive effects. The findings of this experiment would be beneficial to developing stable and efficient supercapacitors, as discussed subsequently.

2. EXPERIMENTAL

2.1 Materials and Chemicals

Analytical reagents and doubly distilled water were used in the experiments. KNO_3 solution (1.0 M) was used as redox-active electrolytes with $K_4[Fe(CN)_6]$ (0.017, 0.033 and 0.050 M). M. YEC-8 AC (0.017, 0.033 and 0.050) characterized by an automatic specific surface area and porosity analyzer (ASAP2020, USA) was provided by Fuzhou Yihuan Co. Ltd. of China. Its physical adsorption of N_2 at 77 K was tested, and the result indicated a type I N_2 isotherm. Thus, this AC was classified as microporous carbon with a specific surface area of 1729 m^2 g^{-1} and an average particle size of 15 mm. The carbon black was provided by Cabot Co. Ltd., USA, and the polytetrafluoroethylene (PTFE) was offered by Dalian Xinyuan Power Stock Co. Ltd., China.

2.2 Electrode Preparation

The AC, carbon black and PTFE were mixed at a mass ratio of 85:10:5. Then, the mixture was dispersed in de-ionized water. After one hour of stirring, a plasticine-like mixture was shaped and then rolled to form a uniform membrane. The carbon-based membrane was then cut into a round sheet (Φ = 10 mm) and pressed onto a current collector (Φ = 13 mm) made of nickel foam. The pressure was 0.6 MPa. Finally, the electrode was dried in an oven at 60 °C for 1 h.

2.3 Properties Characterization

The CV test was carried out in both a three-electrode configuration and a two-electrode capacitor system with a symmetrical configuration. And the EIS test was employed to investigate a three-electrode cell. In the three-electrode configuration, two AC electrodes were used. One of them worked as the working electrode, and the other as the counter electrode. Meanwhile, a reference electrode was made with Ag/AgCl in a saturated KCl solution. In the two-electrode configuration, one electrode with AC was used as the positive electrode, and another with the same AC amount worked as the negative electrode. In the EIS test, the open circuit potential was 0.0 V, the frequency was 10 mHz to 100 kHz, and the voltage amplitude of the applied alternating current signal was 10 mV. To analyze the behavior of each electrode, a T-type Swagelok cell was used to carry out a synchronous charge-discharge process in both the two-electrode capacitor configuration and the three-electrode configuration; the tested current density was 1.0 A g^{-1}. The voltage window of the charge-discharge process was 0-1.5 V.

The CV and EIS tests were carried out in an Advanced Electrochemical System (PARRSTAT 2273, Princeton Applied Research, USA). A battery test system (BTS50V50 mA, Neware Electronic Co. Ltd., China) was used to take the galvanostatic charge-discharge test.

2.4 Parameters

According to Eqs. 1-4., various parameters can be calculated from the charge-discharge curves, including electrode specific capacitance (C_s, F g^{-1}), equivalent series resistance (ESR, Ω), power density (P, W kg^{-1}) and energy density (E, Wh kg^{-1}).

$$C_s = \frac{4 \cdot I \cdot \Delta t}{\Delta V \cdot m_{ac}} \quad (1)$$

$$ESR = \frac{iR_d}{2I} \quad (2)$$

$$P = \frac{I \cdot \Delta V}{2 \cdot m_{ac}} \times \frac{1000}{3600} \quad (3)$$

$$E = \frac{C \cdot \Delta V^2}{2} \times \frac{1000}{3600} \quad (4)$$

where I is the current in the charge-discharge process (A); Δt is the discharge time (s); m_{ac} is the total mass of active materials that are used on the positive and negative electrodes (g); iR_d is the electrical potential difference between the two ends of a conducting phase in the charge-discharge process (V); ΔV is the change of voltage after a whole discharge process (V).

3. RESULTS AND DISCUSSION

3.1 Electrochemical Properties of AC Electrodes

CV curves for AC electrodes in the two configuration setups in the 0.050 M $K_4Fe(CN)_6$ electrolyte and the 1 M KNO_3-0.05 M $K_4Fe(CN)_6$ electrolyte are shown in Fig. 1a. Sharper, larger and narrower redox peaks were obtained in the KNO_3-$K_4[Fe(CN)_6]$ electrolyte than without KNO_3. The difference in peak potential (ΔE_p) of the KNO_3-$K_4[Fe(CN)_6]$ electrolyte was 203 mV. On the contrary, it was only 460 mV for the $K_4[Fe(CN)_6]$. This result showed that electron-transfer kinetics and reversibility of the electrode reactions could be improved by adding KNO_3 in the redox-active $K_4Fe(CN)_6$ electrolyte [21].

Fig. 1b shows the Nyquist plots for AC electrodes in the KNO_3-$K_4Fe(CN)_6$ electrolyte, indicating ideal electrochemical capacitance. The imaginary part of impedance showed a nearly vertical linear feature at the low-frequency region. The intersection point on the x-axis in the range of high frequency indicated that the KNO_3-$K_4Fe(CN)_6$ electrolyte had significantly lower inner resistance (R_s) than $K_4Fe(CN)_6$. Moreover, the span of the semicircle along the x-axis indicated that it had a significantly smaller charge transfer resistance (R_{ct}). Thus, it was reasonable to conclude that adding neutral KNO_3 electrolyte into redox-active $K_4Fe(CN)_6$ can significantly improve the ionic conductivity of the solution, thus benefiting the interfacial interaction between the electrode and the electrolyte.

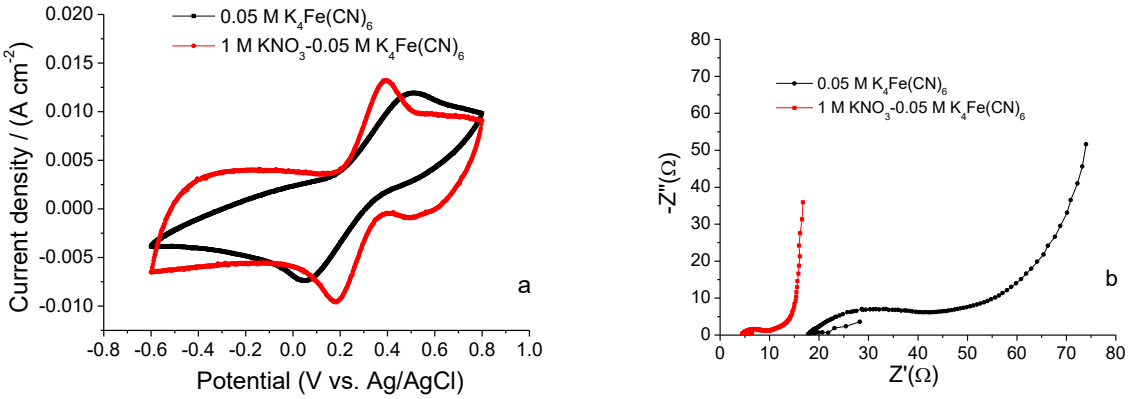

Figure 1. Characterization of AC electrodes in the $K_4[Fe(CN)_6]$ electrolyte and the KNO_3-$K_4[Fe(CN)_6]$ electrolyte in the three-electrode configuration. (a) CVs at a scan rate of 10 mV s^{-1}; (b) EIS.

Fig. 2a shows the CVs in a two-electrode capacitor configuration in the two electrolytes when the voltage window is 0-1.6 V. The CV curve of the KNO_3-$K_4Fe(CN)_6$ electrolyte covered a wider current area. It showed one pair of clear and prominent redox peaks, which indicated redox reactions for the $[Fe(CN)_6]^{4-}$/$[Fe(CN)_6]^{3-}$ couple. In contrast, the CV of the $K_4[Fe(CN)_6]$ electrolyte only showed a relatively small current area, and the redox peaks were not conspicuous. Similarly, the addition of KNO_3 to the $K_4[Fe(CN)_6]$ electrolyte greatly enhanced the capacitive performance due to the high conductivity of the KNO_3 and the consequent acceleration of ions migration and electron-transfer kinetics of redox reactions of the $[Fe(CN)_6]^{4-}$/$[Fe(CN)_6]^{3-}$ couple. In addition, the voltage window was extended up to 1.5 V without water depletion reaction, which was much higher than the 1.0 V reported in the previous studies in acid or alkali electrolytes [22-28]. These results illustrated the merits of this KNO_3-$K_4[Fe(CN)_6]$ electrolyte, which features an enlarged working voltage window in the two-electrode capacitor configuration.

Fig. 2b shows the charge-discharge curves for the two-electrode capacitor configuration obtained in the $K_4Fe(CN)_6$ electrolyte and the KNO_3-$K_4Fe(CN)_6$ electrolyte. The voltage window and current densities were 0-1.5 V and 1 A g^{-1}, respectively. Fig. 2b demonstrates that the curves for both electrolytes exhibit slope variation of the time dependence of potential. This implied pseudocapacitive behaviors caused by the redox reactions of $K_4[Fe(CN)_6]$. On account of the presence of KNO_3, KNO_3-$K_4[Fe(CN)_6]$, electrolyte displays a much longer discharge time and a shorter sharp potential drop in the discharge profiles, which indicated much higher specific capacitance and lower equivalent series resistance than that in $K_4[Fe(CN)_6]$ electrolyte. Parameters according to these charge-discharge curves were calculated by Eqs. 1-4 and listed in Table 1. The specific capacitance (*Cs*), power density (*P*) and energy density (*E*) in the KNO_3-$K_4[Fe(CN)_6]$ electrolyte were 250 F g^{-1}, 332 W kg^{-1} and 14.4 Wh kg^{-1}, respectively. Such values were much higher than those in the controls of 0.050 M $K_4[Fe(CN)_6]$ electrolyte, which were 106 F g^{-1}, 268 W kg^{-1} and 4.3 Wh kg^{-1}, respectively. These values were also higher than that in the previous reports when only $K_4[Fe(CN)_6]$ or $K_4[Fe(CN)_6]$ incorporated with acid or alkaline electrolytes were used [11,29], and they were well explained by the wider voltage window of 1.5 V resulting from the introduction of KNO_3.

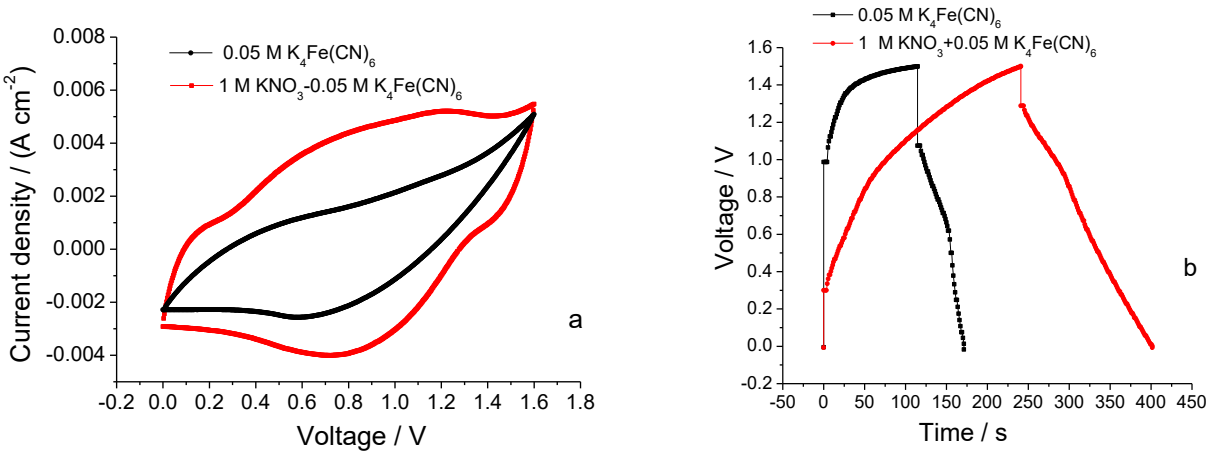

Figure 2. Characterization of the AC-AC symmetric capacitors in the $K_4[Fe(CN)_6]$ electrolyte and KNO_3-$K_4[Fe(CN)_6]$ electrolyte (two-electrode configuration). (a) CVs at a scan rate of 10 mV s^{-1}; (b) galvanostatic charge-discharge curves.

Table 1. Parameter values derived from the calculation on the feature points of the charge-discharge curves of AC-AC symmetric capacitor in the $K_4[Fe(CN)_6]$ electrolyte and the KNO_3-$K_4[Fe(CN)_6]$ electrolytes in the two-electrode configuration.

Electrolyte	C_s (F g^{-1})	*ESR*	P (W kg^{-1})	E (Wh kg^{-1})
0.050 M $K_4[Fe(CN)_6]$	106	60.1	268	4.3
1 M KNO_3-0.050 M $K_4[Fe(CN)_6]$	250	29.6	332	14.4
1 M KNO_3-0.033 M $K_4[Fe(CN)_6]$	227	30.4	321	13.0
1 M KNO_3-0.017 M $K_4[Fe(CN)_6]$	201	31.7	319	11.4

Fig. 3a shows representative CV curves obtained when a three-electrode configuration is used in the KNO_3-$K_4Fe(CN)_6$ electrolyte under scan potentials ranging from -0.6 to 0.8 V vs. Ag/AgCl. A well-defined pair of Faradaic peaks at E_{pa} of 0.32 V (vs. Ag/AgCl) and E_{pc} of 0.19 V (vs. Ag/AgCl) at a scan rate of 10 mV s^{-1} characterized the voltammetric profiles, which are assigned to the reversible reaction equation involving electron transfer process, as shown in the following Eq. 5:

$$Fe(CN)_6^{3-} + e^- \longleftrightarrow Fe(CN)_6^- \quad (5)$$

Fig. 3b and 3c show a linear interrelation between the peak currents (i_{pa} and i_{pc}) and the square root of the scan rate ($v^{1/2}$). This strongly demonstrated that diffusion-controlled oxidation/reduction took place in the for $[Fe(CN)_6]^{4-}$/$[Fe(CN)_6]^{3-}$ couple. Moreover, both the peak redox current and the peak potential separation increased along with the scanning rate, which further confirmed the existence of the diffusion-controlled reaction.

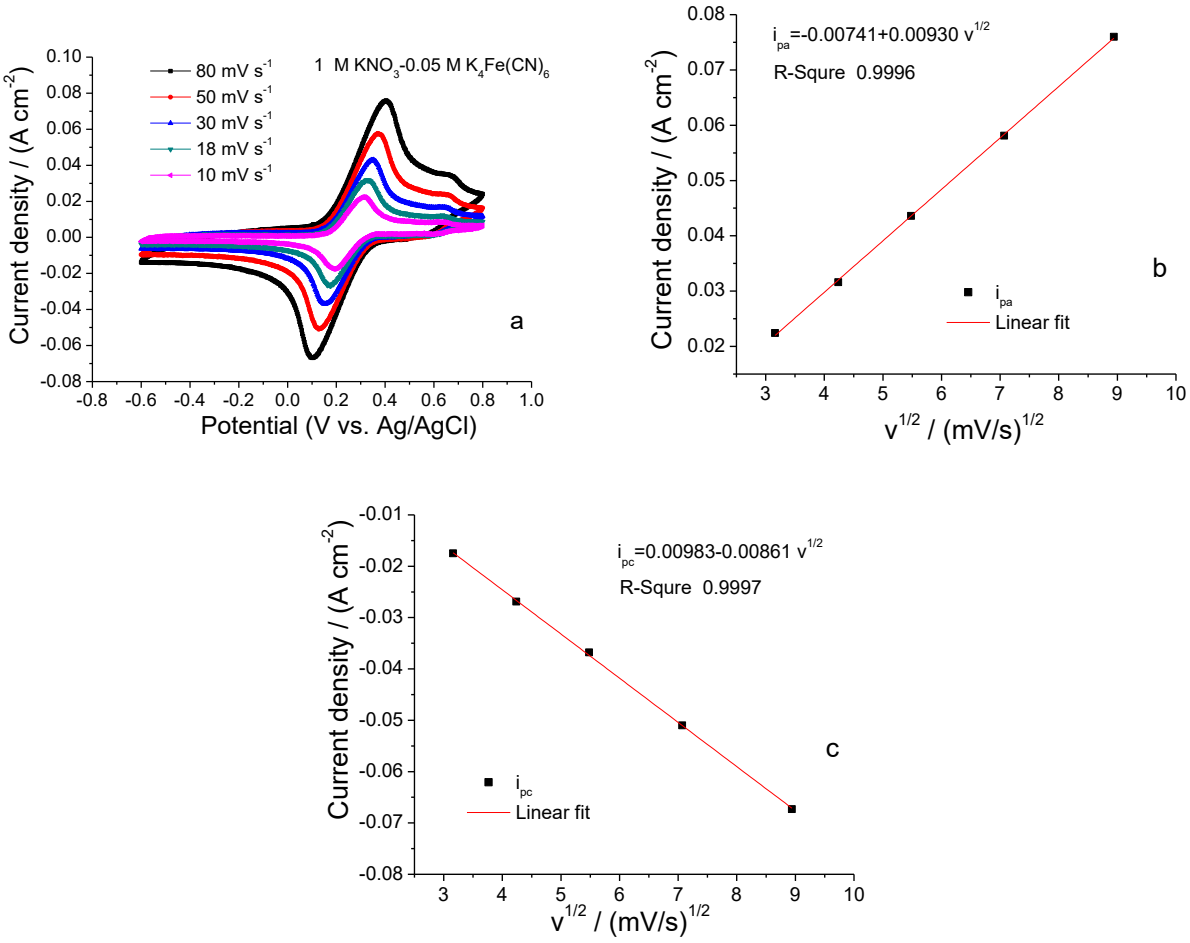

Figure 3. Characterization of AC electrode in the KNO_3-$K_4[Fe(CN)_6]$ electrolytes (three-electrode configuration). (a) CVs at various scan rates in the range of 10-80 mV s^{-1} ; (b) linear fitting between the anodic peak current and the square root of the scan rate; (c) linear fitting between the cathodic peak current and the square root of the scan rate.

Effects of $K_4[Fe(CN)_6]$ have been widely concerned in the research field and industry. Ali et al. used a standard solution of 0.06 mM $K_4[Fe(CN)_6]$ in 0.1 M KCl as an electrolyte and studied the Fe(II)/Fe(III) redox current peaks at various concentrations, pH values, scan rates. They found the new modified electrode's reversible and heterogeneous reaction in the electrolyte. Subsequently, they revealed that the new nanoscale sensor has a low detection limit due to nanoparticles' good reliability and stability and better oxidation-reduction current peaks in an acidic medium [30]. Arunpandiyan achieved better electrochemical performance by using a reversible redox reaction involving 0.2 M $K_4[Fe(CN)_6]$, and the energy and power density reached 39.6 W h $kg^{-1}$and 550 W kg^{-1}, respectively[31].

3.2 Effect of the $K_4[Fe(CN)_6]$ Concentration on the KNO_3-$K_4Fe(CN)_6$ Electrolytes

To investigate the effect of $K_4Fe(CN)_6$ concentration in the KNO_3-$K_4Fe(CN)_6$ electrolyte on electrode capacitive performance, CV curves in three different conditions were drawn. The three-

electrode configuration was used. The electrodes were immersed in electrolytes of 1 M KNO_3 incorporated with 0.017, 0.033 and 0.050 M $K_4[Fe(CN)_6]$, respectively. Characteristic peaks of the curve assigned to Faradic reactions of $[Fe(CN)_6]^{4-}/[Fe(CN)_6]^{3-}$ couple are shown in Fig. 4a. According to the enhanced capacitance, the redox peak current increased significantly along with the K4[Fe(CN)6] concentration.

Fig. 4b shows the EIS in electrolytes of 1 M KNO_3 incorporated with 0.017, 0.033 and 0.050 M $K_4[Fe(CN)_6]$ when a three-electrode configuration was used. The intersection points at the high-frequency range on the real axis indicated that the bulk resistance (R_s) decreased with $K_4[Fe(CN)_6]$ concentration. In the Nyquist plots, the diameter of the semicircle in the medium-high frequency range indicated that the charge transfer resistance (R_{ct}) decreased when the $K_4[Fe(CN)_6]$ concentration increased. Bulk resistance and charge-transfer resistance of the AC electrodes in an electrolyte with high $K_4[Fe(CN)_6]$ concentration had dropped, resulting in lower internal resistance of the supercapacitor.

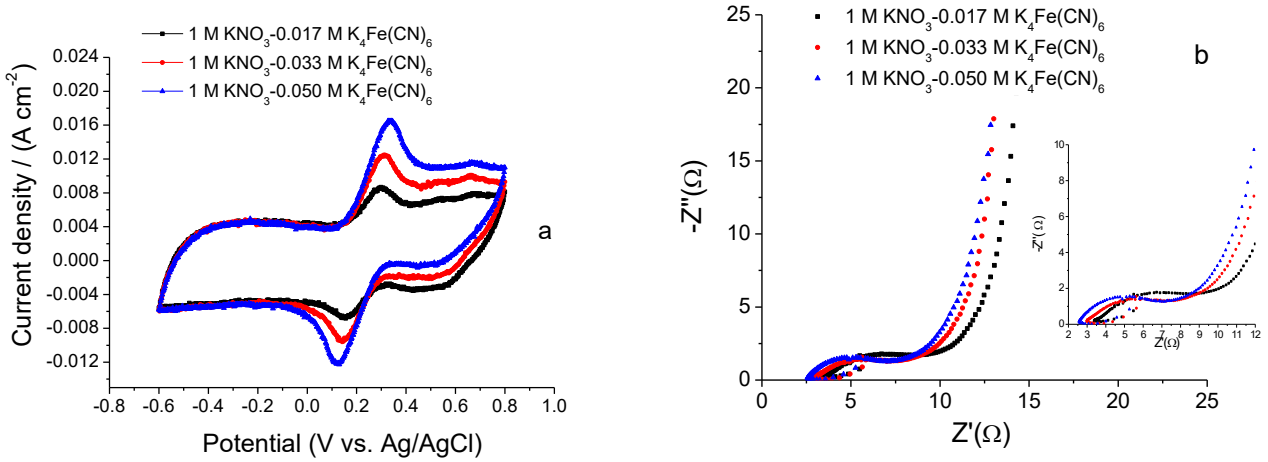

Figure 4. Characterization of AC electrodes in KNO_3 electrolytes with different $K_4[Fe(CN)_6]$ concentrations (three-electrode configuration). (a) CVs at a scan rate of 10 mV s^{-1}; (b) EIS.

A typical pseudocapacitive behavior during the galvanostatic charge/discharge cycling tests is exhibited in Fig. 5a, where a slope variation appears on the potential's time dependence curves. Higher concentrations of $K_4[Fe(CN)_6]$ led to extended charge-discharge time, indicating higher capacitance values. This trend was well consistent with the CVs in Fig. 4a. The sharp potential drop in the discharge profiles indicated that the internal resistance decreased when $K_4[Fe(CN)_6]$ concentration increased, illustrating that high $K_4[Fe(CN)_6]$ concentrations were responsible for higher solution conductivity and the consequent lower internal resistances. This result was consistent with that in Fig. 4b.

To evaluate the behaviors of electrodes in KNO_3-$K_4[Fe(CN)_6]$ electrolytes, synchronous experiments in a three-electrode configuration were carried out. The galvanostatic charge/discharge cycles changed from 0 to 1.5 V. The evolution of potentials of the positive and negative electrodes is shown in Fig. 5b. The potential windows of the positive electrode and the negative electrode (vs. Ag/AgCl electrode) in 1 M KNO_3-0.050 M $K_4[Fe(CN)_6]$ were -0.29 to 0.33 V and -0.29 to -1.17 V when

the supercapacitor was charged from 0 to 1.5 V. They were -0.32 to 0.32 V and -0.32 to -1.18 V in the 1 M KNO_3-0.033 M $K_4[Fe(CN)_6]$ electrolyte, and -0.38 to 0.29 V and -0.38 to -1.21 V in 1 M KNO_3-0.017 M $K_4[Fe(CN)_6]$ electrolyte. The charge-discharge curves of the negative electrode were linear, and some distortions indicated the redox processes on the positive electrode, which verified that redox reactions took place on the positive electrode. This result was consistent with the CVs in Fig. 4a, where a pair of Faradaic peaks indicating the redox reactions of the $[Fe(CN)_6]^{4-}/[Fe(CN)_6]^{3-}$ couple appeared within the AC positive electrode potential window.

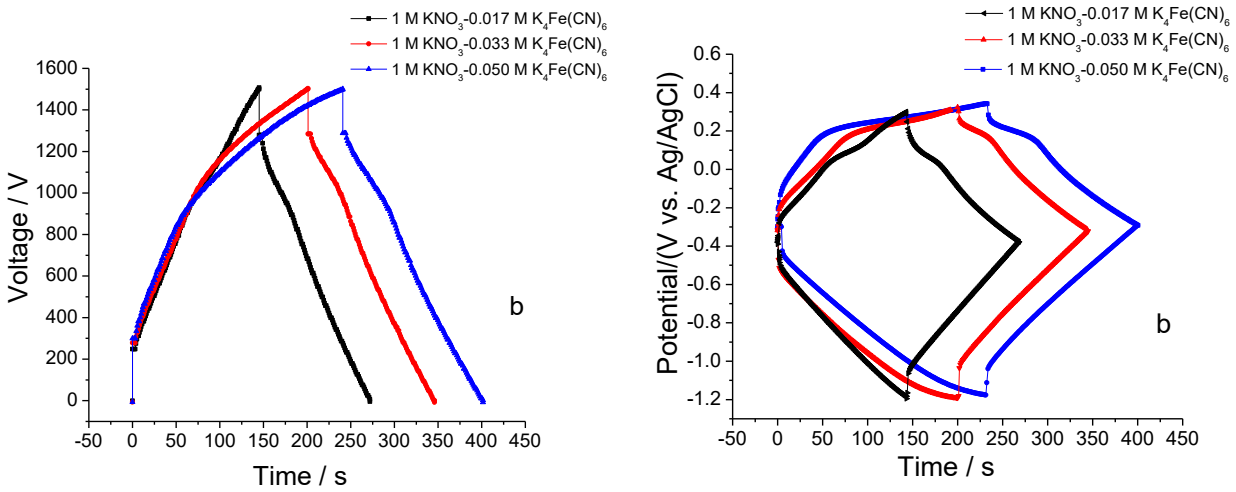

Figure 5. Charge-discharge curves of two systems in KNO_3 electrolytes with different $K_4[Fe(CN)_6]$ concentration when the cell voltage range is 0-1.5 V, and the current density is 1 A g^{-1}. (a) AC-AC symmetric capacitor in the two-electrode configuration; (b) positive AC electrode and negative AC electrode in the three-electrode configuration

Fig. 4a shows that redox reactions of the $[Fe(CN)_6]^{4-}/[Fe(CN)_6]^{3-}$ couple can be accomplished in a three-electrode configuration when the potential window is -0.1 to 0.5 V (vs. Ag/AgCl). However, the situation changed significantly if a two-electrode capacitor configuration was used. As the cell voltage changed from 0 to 1.5 V during the charge-discharge processes, the potential windows in various electrolytes were limited to -0.29 to 0.33 V, -0.32 to 0.32 V and -0.38 to 0.29 V when the concentration of $K_4[Fe(CN)_6]$ was 0.050, 0.033 and 0.017 M, respectively. This indicated that the redox reactions of $Fe(CN)_6^{4-}/Fe(CN)_6^{3-}$ could not be fully completed in a two-electrode capacitor configuration. However, it still significantly improved the capacitor's electrochemical properties (Table 1). The *Cs*, *ESR*, *P* and *E* at various $K_4[Fe(CN)_6]$ concentrations demonstrated that KNO_3 incorporated with higher concentrations of $K_4[Fe(CN)_6]$ could lead to higher *Cs*, *P* and *E*, and lower *ESR*. The maximum *Cs*, *P* and *E* reached 250 F g^{-1}, 332 W kg^{-1} and 14.4 Wh kg^{-1} in 1 M KNO_3-0.050 M $K_4[Fe(CN)_6]$.

Fig. 6a shows that, when the voltage window is 0 to 1.6 V, CVs in two-electrode capacitor configuration in KNO_3 incorporated with different $K_4[Fe(CN)_6]$ concentrations exhibit characteristic peaks assigned to Faradic reactions. Redox peak currents increased with the $K_4[Fe(CN)_6]$ concentration, indicating that redox-active $K_4[Fe(CN)_6]$ positively enhanced the capacitive properties. This result

obtained in the two-electrode configuration corresponded with that in the three-electrode configuration shown in Fig. 4a.

Fig. 6b shows the charge/discharge cyclic stability when the two-electrode capacitor configuration is employed. The capacitor's highest capacitance and worst cyclic stability were obtained when the $K_4[Fe(CN)_6]$ concentration reached its maximum value. On the contrary, the lowest capacitance and the best cyclic stability were obtained when the $K_4[Fe(CN)_6]$ concentration reached its minimum value. The capacitance losses were 28.6%, 9.8% and 4.5% when the concentration of $K_4[Fe(CN)_6]$ was 0.050, 0.033 and 0.017 M, respectively. Redox reactions and the consequent specific capacitance decreased along with the $K_4[Fe(CN)_6]$ concentration. However, a high $K_4[Fe(CN)_6]$ concentration can lead to an increase in concentration polarization, resulting in poorer electrochemical stability [32,33]. Balance among energy density, power density and cycle life was expected to be achieved when a proper $K_4[Fe(CN)_6]$ concentration was used. Among the three neutral electrolytes with different $K_4[Fe(CN)_6]$ concentrations, 1 M KNO_3-0.033 M $K_4[Fe(CN)_6]$ exhibited a proper capacitive property with 227 F g^{-1} *Cs*, 321 W kg^{-1} *P*, and 13.0 Wh kg^{-1} *E*.

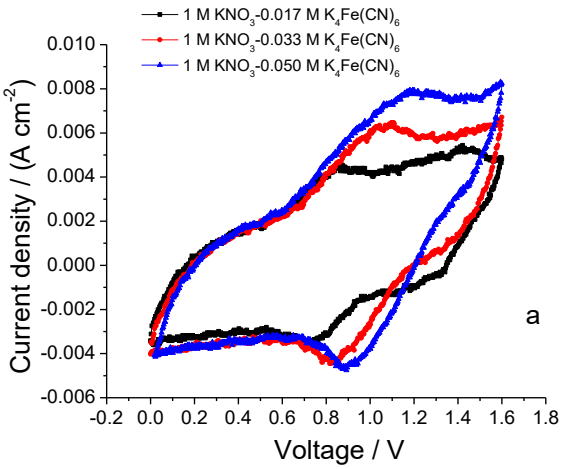

Figure 6. Characterization of the AC-AC symmetric capacitor in electrolytes of KNO_3 with different $K_4[Fe(CN)_6]$ concentrations in the two-electrode configuration). (a) CVs at a scan rate of 20 mV s^{-1}; (b) variations of specific capacitances with cycle number at a current density of 1 A g^{-1}.

Tian et al. introduced $K_4Fe(CN)_6$ as a redox additive into the neutral medium of KNO_3 and reported that in 2 M KNO_3-0.017 M $K_4[Fe(CN)_6]$ at 1 A g^{-1}, the Cs, P and E reached 159 F g^{-1}, 525 W kg^{-1} and 17.3 Wh kg^{-1}. The Cs was lower than this study, while the other two indicators were higher. This difference may be explained by the vairous concentrations of KNO_3 and $K_4[Fe(CN)_6]$ [34].

Pareek et al. synthesized 3D graphene electrodes for microbial fuel cells and used cyclic voltammetry and Nyquist plots to characterize their performance. They found the maximum power density in potassium ferricyanide was 36% higher than that in MFC-DO and 44% higher than that in MFC-NDO. Our research found that increasing the density of potassium ferricyanide can further increase

power density. Therefore, it is highly worthy to further develop activated carbon electrodes with advanced structures combining potassium ferricyanide [35].

4. CONCLUSIONS

Neutral KNO_3 electrolyte incorporated with $K_4[Fe(CN)_6]$ successfully extended the voltage window of symmetric AC-AC capacitor and enhanced its capacitance. The maximum specific capacitance, power density and energy density were 250 F g^{-1}, 332 W kg^{-1} and 14.4 Wh kg^{-1}, respectively, when 1 M KNO_3-0.050 M $K_4Fe(CN)_6$ was used, despite the incomplete redox reactions of $[Fe(CN)_6]^{4-}$/$[Fe(CN)_6]^{3-}$. Higher $K_4[Fe(CN)_6]$ concentration led to higher capacitance and lower cyclic stability. A proper $K_4[Fe(CN)_6]$ concentration incorporated with KNO_3 was thus expected to simultaneously achieve a balance among high energy density, high power density and acceptable cycle life. This study achieved the most favorable balance when the $K_4[Fe(CN)_6]$ concentration was 0.033 M.

The application of $K_4[Fe(CN)_6]$ can also be further expanded in the future; for example, Radhi proposed a novel glassy carbon electrode with a standard solution of 1 mM $K_4[Fe(CN)_6]$ with 1 M K_2HPO_4 as an electrolyte [36]. In the future, the KNO_3-$K_4[Fe(CN)_6]$ solution is expected to be used for similar solutions.

FUNDING STATEMENT
This research is supported by the Natural Science Foundation of China (No.21377019, 51578104 and 21273025).

CONFLICTS OF INTEREST
The authors declare that they have no competing interests.

DATA AVAILABILITY STATEMENT
The data used to support the findings of this study are included within the article.

References

1. J. T. Li, W. Zhao, F. Q. Huang, A. Manivannan, N. Q. Wu, *Nanoscale,* 3 (2011) 5103.
2. D. L. Fang, Z. D. Chen, X. Li, Z. F. Wu, C. H. Zhang, *Electrochim. Acta,* 81 (2012) 321.
3. Y. H. Ko, S. Kim, J. S. Yu, *Mater. Lett*., 84 (2012) 132.
4. D. Qu, *J. Power Sources,* 109 (2002) 403.
5. W. Li, F. Zhang, Y. Q. Dou, Z. X. Wu, H. J. Liu, X. F. Qian, D. Gu, Y. Y. Xia, *Adv. Energy Mater*., 1 (2011) 382.
6. C. T. Hsieh, H. Teng, *Carbon*, 40 (2002) 667.
7. W. R. Li, D. H. Chen, Z. Li, Y. F. Shi, Y. Wan, G. Wang, Z. Y. Jiang, D. Y. Zhao, *Carbon,* 45 (2007) 1757.
8. C. H. A. Wong, A. Ambrosi, M. Pumera, *Nanoscale,* 4 (2012) 4972.
9. Cheng P Z, Teng H, *Carbon,* 41 (2003) 2057.
10. C. C. Hu, C. C. Wang, *J. Power Sources,* 125 (2004) 299.
11. L. H. Su, X. G. Zhang, C. H. Mi, B. Gao, Y. Liu, *Phys. Chem. Chem. Phys*., 11 (2009) 2195.

12. C. Zhao, W. Zheng, X. Wang, H. Zhang, X. Cui, H. Wang, *Sci. Rep*., 3 (2013) 2986.
13. A. Shanumgavani, S. Kaviselvi, K. V. Sankar, R. K. Selvan, *Mater. Res. Bull*., 62 (2015) 161.
14. Y. M. Wang, J. Y. Cao, Y. Zhou, J. H. Ouyang, D. C. Jia, L. X. Guo, *J. Electrochem. Soc*., 159 (2012) A579.
15. X. Yang, Y. S. He, G. Jiang, X. Z. Liao, Z. F. Ma, *Electrochem. Commun*., 13 (2011) 1166.
16. K. Karthikeyan, D. Kalpana, S. Amaresh, Y. S. Lee, *RSC Adv,*. 2 (2012) 12322.
17. L. Demarconnay, R. P. Beguin, *Electrochim. Commun*., 12 (2010) 1275.
18. Y.-K. Ksu, Y.-C. Chen, Y.-G. Lin, L.-C. Chen, K.-H. Chen, *J. Mater. Chem*., 22 (2012) 3383.
19. L. Zhao, J. Yu, W. Li, S. Wang, C. Dai, J. Wu, X. Bai, C. Zhi, *Nano Energy,* 4 (2014) 39.
20. J. Cao, Y. Wang, Y. Zhou, J.-H. Ouyang, D. Jia, L. Guo, *J. Electroanal. Chem*., 689 (2013) 201.
21. J. Wang, U. A. Kirgoz, J. W. Mo, J. M. Lu, A. N. Kawade, A. Muck, *Electrochem. Commun*., 3 (2001) 203.
22. S. Roldan, M. Granda, R. Menendez, R. Santamaria, C. Blanco, *J. Phys. Chem*., C 115 (2011) 17606.
23. S. Roldan, Z. Gonzalez, C. Blanco, M. Granda, R. Menendez, R. Santamaria, *Electrochim. Acta,* 56 (2011) 3401.
24. S. Roldan, M. Granda, R. Menendez, R. Sntamaria, C. Blanco, *Electrochim. Acta,* 83 (2012) 241.
25. J. Wu, H. Yu, L. Fan, G. Luo, J. Lin, M. Huang, *J. Mater. Chem*., 22 (2012) 19025.
26. W. Chen, R. B. Rakhi, H. N. Alshareef, *Nanoscale,* 3 (2013) 4134.
27. K. B. Hatzell, M. Beidaghi, J. W. Campos, C. R. Dennison, E. C. Kumbur, Y. Gogotsi, *Electrochim. Acta,* 111 (2013) 888.
28. P. Diaz, Z. Gonzalez, R. Santamaria, M. Granda, R. Menendez, *Electrochim. Acta,* 168 (2015) 277.
29. K. V. Sankar, R. K. Selvan, *Carbon,* 90 (2015) 260.
30. A. N. Lafta, M. M. Radhi, A. A. Mossa, *Adv. Nano. BioM&D.*, 4 (2020) 603 ‑ 616.
31. S. Arunpandiyan, A. Raja, S. Vinoth, A. Pandikumar, A. Arivarasan, *New J. Chem.*, 45 (2021) 12808.
32. Y. Tian, J. W. Yan, R. Xue, B. L. Yi, *J. Electrochem. Soc*., 158 (2011) A818.
33. S. T. Senthikumar, R. Kalaiselvan, Y. S. Lee, J. S. Melco, *J. Mater. Chem*., A 1 (2013) 1086.
34. Y. Tian, M. Liu, R. Che, R. Xue, L. Huang, *J. Power Sources,* 324 (2016) 334–341.
35. A. Pareek, J.S. Sravan, S. V Mohan, *Carbon Resour. Convers.*, 2 (2019) 134–140.
36. M. M. Radhi, A. A. Moosa, I. A. Khalaf, *Nano Biomed. Eng.*, 10 (2018) 10-15.